Report

Cell Reports

A constant pool of Lgr5$^+$ intestinal stem cells is required for intestinal homeostasis

Graphical Abstract

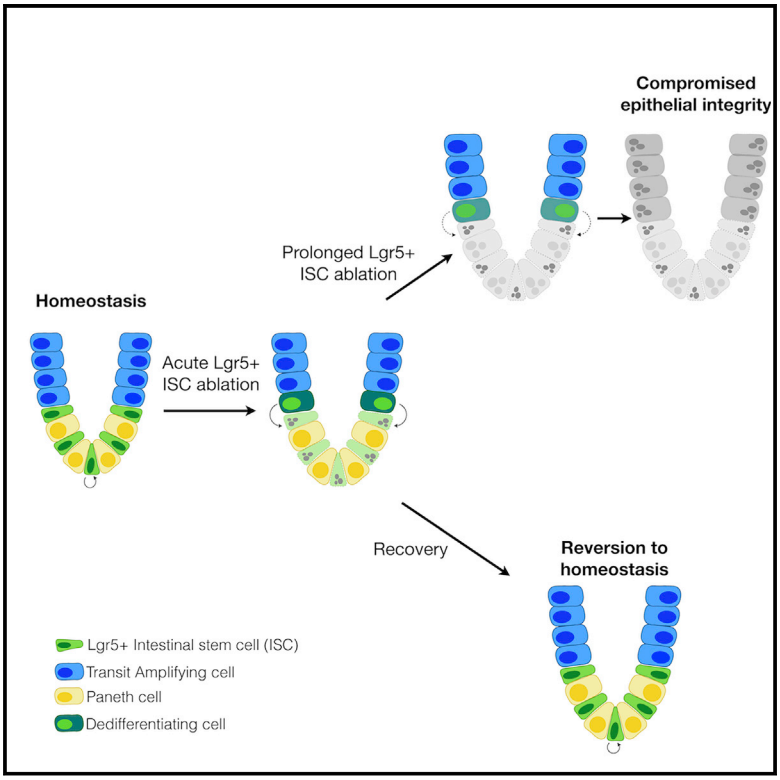

Highlights

- Persistent depletion of Lgr5$^+$ ISCs compromises epithelial integrity *in vivo*
- Lgr5$^+$ ISC ablation precludes organoid formation and maintenance *in vitro*
- 2A models retain wild-type Lgr5 levels and enable compound Lgr5 reporter mice
- Lgr5-2A-DTR model ablates Lgr5$^+$ ISCs more efficiently than Lgr5-DTR-EGFP model

Authors

Si Hui Tan, Phyllis Phuah, Liang Thing Tan, ..., Esther Wong, Bernett Lee, Nick Barker

Correspondence

nicholas_barker@imcb.a-star.edu.sg

In Brief

Lgr5$^+$ intestinal stem cells are thought to be dispensable for intestinal homeostasis. Using a sensitive Lgr5-2A-DTR model, Tan et al. show that the constant depletion of these Lgr5$^+$ cells in fact compromises intestinal epithelial integrity *in vivo* and precludes organoid growth *in vitro*.

Tan et al., 2021, Cell Reports *34*, 108633
January 26, 2021
https://doi.org/10.1016/j.celrep.2020.108633

CellPress

Cell Reports

CellPress
OPEN ACCESS

Report

A constant pool of Lgr5$^+$ intestinal stem cells is required for intestinal homeostasis

Si Hui Tan,[1,2] Phyllis Phuah,[1,3] Liang Thing Tan,[1,2] Swathi Yada,[1,2] Jasmine Goh,[1,4] Lucian B. Tomaz,[5] Magdalene Chua,[6] Esther Wong,[1,2] Bernett Lee,[7] and Nick Barker[1,2,8,9,*]

[1]A*STAR Institute of Medical Biology, Singapore, Singapore
[2]A*STAR Institute of Molecular and Cell Biology, Singapore, Singapore
[3]Section of Endocrinology & Investigative Medicine, Department of Metabolism, Digestion, and Reproduction, Imperial College London, London, UK
[4]Cancer Science Institute, Singapore, Singapore
[5]Lee Kong Chian School of Medicine, Nanyang Technological University, Singapore, Singapore
[6]School of Biological Sciences, Nanyang Technological University, Singapore, Singapore
[7]A*STAR Singapore Immunology Network, Singapore, Singapore
[8]Division of Epithelial Stem Cell Biology, Cancer Research Institute, Kanazawa University, Kanazawa, Japan
[9]Lead contact
*Correspondence: nicholas_barker@imcb.a-star.edu.sg
https://doi.org/10.1016/j.celrep.2020.108633

SUMMARY

Lgr5$^+$ crypt base columnar cells, the operational intestinal stem cells (ISCs), are thought to be dispensable for small intestinal (SI) homeostasis. Using a Lgr5-2A-DTR (diphtheria toxin receptor) model, which ablates Lgr5$^+$ cells with near-complete efficiency and retains endogenous levels of Lgr5 expression, we show that persistent depletion of Lgr5$^+$ ISCs in fact compromises SI epithelial integrity and reduces epithelial turnover *in vivo*. *In vitro*, Lgr5-2A-DTR SI organoids are unable to establish or survive when Lgr5$^+$ ISCs are continuously eliminated by adding DT to the media. However, transient exposure to DT at the start of culture allows organoids to form, and the rate of outgrowth reduces with the increasing length of DT presence. Our results indicate that intestinal homeostasis requires a constant pool of Lgr5$^+$ ISCs, which is supplied by rapidly reprogrammed non-Lgr5$^+$ crypt populations when preexisting Lgr5$^+$ ISCs are ablated.

INTRODUCTION

As one of the most rapidly renewing organs, small intestine (SI) crypts display remarkable plasticity. Lgr5$^+$ crypt base columnar cells (CBCs) are intestinal stem cells (ISCs) that fuel homeostatic epithelium renewal (Barker et al., 2007). When Lgr5$^+$ ISCs are acutely ablated, the population is rapidly regenerated from other crypt populations, such as Bmi1$^+$ "reserve" stem cells, secretory progenitors, enterocyte progenitors, and/or Paneth cells (Jones et al., 2019; Schmitt et al., 2018; Tetteh et al., 2016; Tian et al., 2011; van Es et al., 2012; Yu et al., 2018), thereby preserving the SI integrity and function critical for survival.

Ablation of Lgr5$^+$ ISCs expressing diphtheria toxin receptor (DTR) using an established Lgr5-DTR-EGFP mouse model (hemizygous for Lgr5 knockin allele) (Figure 1A) causes no obvious phenotype using an alternate day DT dosing regimen, leading to the conclusion that Lgr5$^+$ ISCs are dispensable for homeostasis (Tian et al., 2011). This study reported that Bmi1$^+$ "reserve" stem cells proliferated to compensate for the loss of Lgr5$^+$ ISCs, thus maintaining homeostasis. However, it was recently shown that replenishment of ablated Lgr5$^+$ ISCs is mainly attributed to Ascl2-dependent dedifferentiation of recent Lgr5$^+$ progeny, with little contribution from older crypt cells, including "reserve" stem cells (Murata et al., 2020). Furthermore, SI integrity in *Ascl2*$^{-/-}$ mice was compromised when dedifferentiation into Lgr5$^+$ ISCs was blocked (Murata et al., 2020). Here, we support and extend the findings that a constant Lgr5$^+$ ISC pool is required for maintaining healthy SI epithelium.

Using Lgr5-2A-DTR (Seishima et al., 2019) and Lgr5-2A-CreERT2 (Leushacke et al., 2017) mouse models that retain wild-type (WT) *Lgr5* expression levels, we show that blocking the re-establishment of Lgr5$^+$ ISCs via daily ablation compromises intestinal integrity. Using an *in vitro* epithelial-only organoid system, we confirm that the *in vivo* phenotype is a direct consequence of losing Lgr5$^+$ ISCs, because Lgr5$^+$ ISCs are required for organoid initiation and survival. Therefore, a constant pool of Lgr5$^+$ ISCs, regardless of whether they preexist or are newly derived from other populations, is necessary for maintaining intestinal homeostasis. The conclusion that Lgr5$^+$ ISCs are dispensable for homeostasis in earlier publications was likely a consequence of incomplete Lgr5$^+$ ISC ablation using the Lgr5-DTR-EGFP allele.

RESULTS

Lgr5-2A-DTR mouse model retains endogenous Lgr5 expression levels and efficiently ablates Lgr5 ISCs

To efficiently ablate Lgr5$^+$ cells, we generated an Lgr5-2A-DTR mouse model in which a DTR cassette is inserted immediately

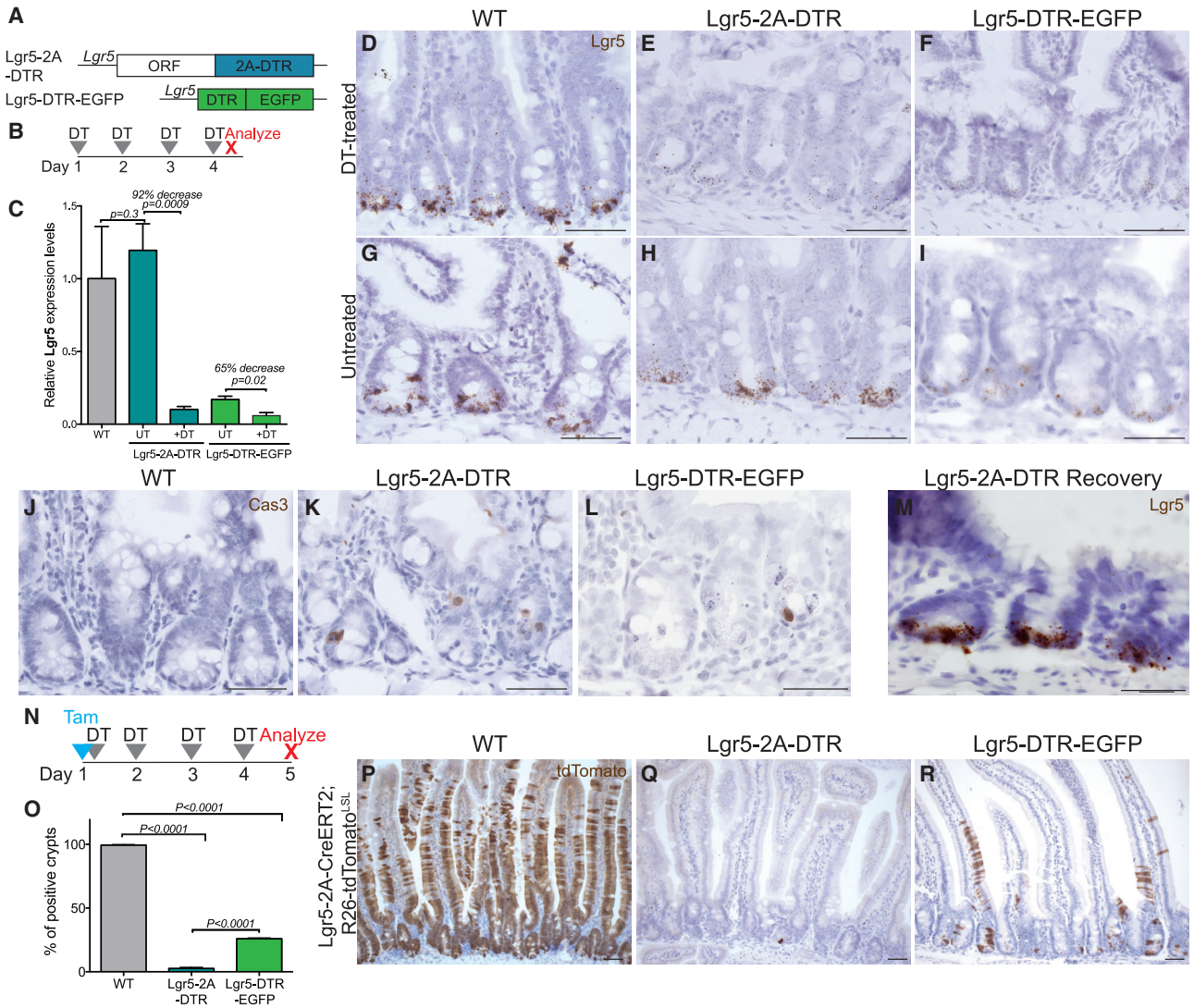

Figure 1. Lgr5-2A-DTR maintains endogenous Lgr5 expression and facilitates efficient DT-mediated Lgr5$^+$ cell ablation *in vivo*

(A) Schematic of Lgr5-2A-DTR and Lgr5-DTR-EGFP constructs.

(B) Experimental timeline for (C)–(I).

(C–I) Lgr5 mRNA expression from untreated and DT-treated WT, Lgr5-2A-DTR, Lgr5-DTR-EGFP proximal SI by qPCR (C), and RNA *in situ* hybridization (ISH) (D–I) (n = 3–4/condition).

(J–L) Representative images of activated caspase 3 staining in WT (J), Lgr5-2A-DTR (K), and Lgr5-DTR-EGFP (L) crypts.

(M) Lgr5 ISH in crypts of Lgr5-2A-DTR mice given DT on 2 consecutive days, and harvested 4 days after the second dose (n = 3).

(N) Experimental timeline for (O)–(R).

(O) Quantification of proportion of proximal SI crypts with ≥2 dTom$^+$ adjacent cells in the upper half of the crypt (n = 3/group, >100 crypts per mouse).

(P–R) Representative images of dTom staining in WT (P), Lgr5-2A-DTR (Q), and Lgr5-DTR-EGFP (R) proximal SI.

Scale bars represent 50 μm. Error bars represent SEMs.

before the endogenous stop codon of Lgr5, and is linked to the *Lgr5* ORF with a 2A peptide, resulting in an Lgr5-2A-DTR fusion protein (Figure 1A). The 2A peptide then automatically self-cleaves to yield two functional proteins—Lgr5 and DTR. Unlike earlier Lgr5-reporter alleles, the 2A model retains endogenous *Lgr5* expression, facilitating the generation of compound mouse models harboring both Lgr5-2A-DTR and Lgr5-reporter/tracing alleles while circumventing the neonatal lethality that would otherwise occur in *Lgr5* knockouts (Barker et al., 2007; Tian et al., 2011).

Control Lgr5-2A-DTR SI expressed *Lgr5* mRNA at similar levels to that of WT (119% ± 18% of WT levels) (Figure 1C), whereas Lgr5 expression was substantially reduced in SI from Lgr5-DTR-EGFP (17% ± 2% of WT levels) and Lgr5-EGFP-ires-CreERT2 models (Figures 1A, 1C, and S1A; Barker et al., 2007; Tian et al., 2011), likely due to the Lgr5 hemizygosity resulting from the targeted introduction of the reporter cassettes, and confirmed by RNA *in situ* hybridization (ISH) (Figures 1G–1I). DTR expression, like Lgr5, was restricted to all crypt bases in

CellPress
OPEN ACCESS

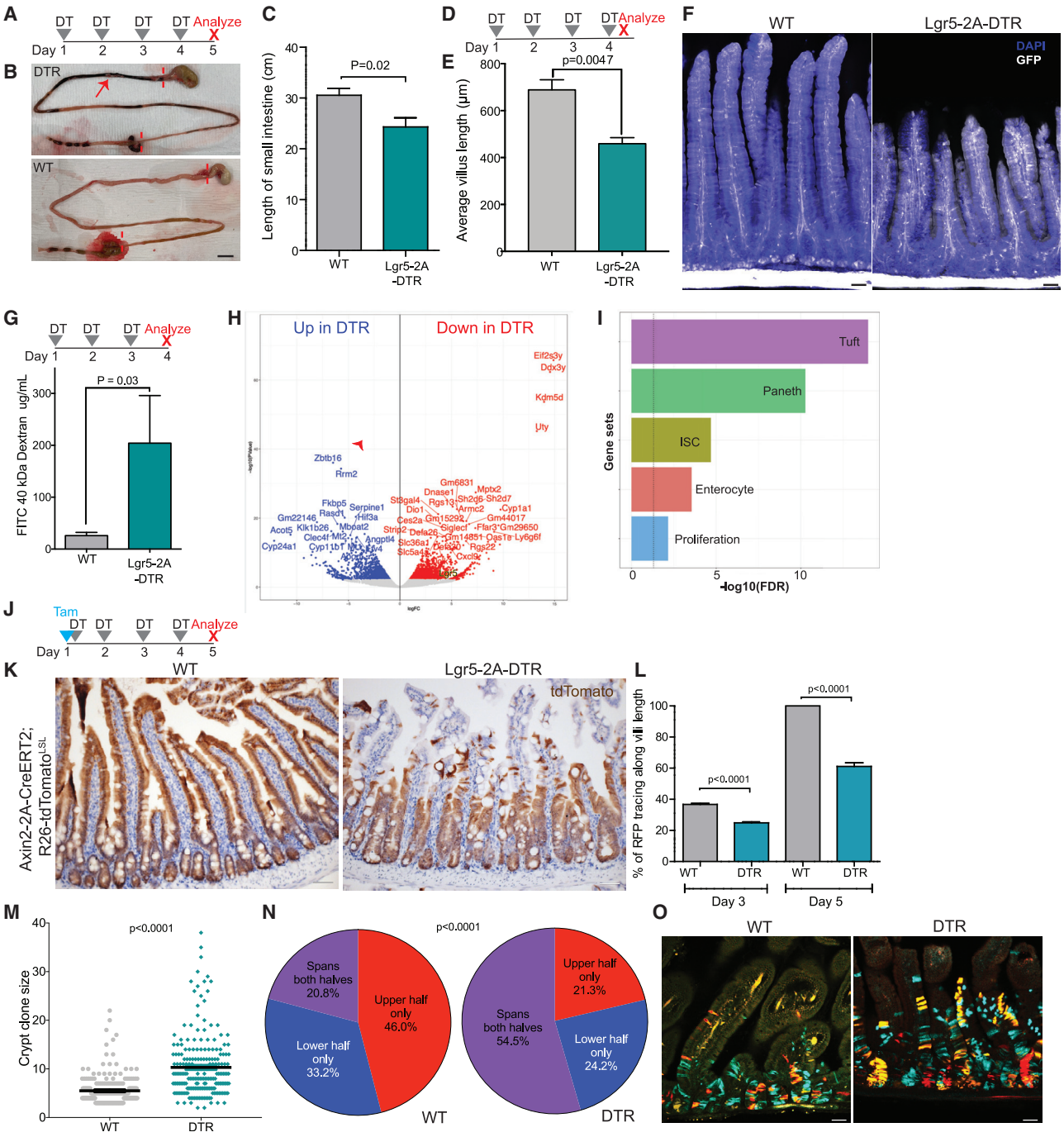

Figure 2. Ablation of Lgr5^{+} ISCs in Lgr5-2A-DTR results in multiple SI phenotypes

(A) Experimental timeline for (B) and (C).

(B) Representative images of DT-treated WT and Lgr5-2A-DTR SI. The red dashes denote the length of SI, and the red arrow points to a hemorrhage in SI.

(C) Lengths of DT-treated WT and Lgr5-2A-DTR SI (n = 6 mice/group).

(D) Experimental timeline for (E) and (F) and (H) and (I).

(E) Average villi lengths from WT (n = 3) and Lgr5-2A-DTR (n = 4).

(F) Representative images of villi from whole-mount WT and Lgr5-2A-DTR SI. Statistics analyzed by Mann-Whitney test.

(G) Experimental timeline for intestinal permeability assay with fluorescein isothiocyanate (FITC)-conjugated 40 kDa dextran on DT-treated WT and Lgr5-2A-DTR SI (n = 4/group).

(H) Volcano plot of differentially expressed genes between DT-treated WT and Lgr5-2A-DTR SI (n = 3/group).

(I) Overrepresentation analysis of markers for various SI epithelial populations and proliferation markers.

(legend continued on next page)

Lgr5-2A-DTR and Lgr5-DTR-EGFP models by ISH, with the latter expressing less DTR (Figure S1B). Hence, the 2A models faithfully recapitulate endogenous Lgr5 expression in the SI, making them physiologically more accurate than existing exon1-knockin models.

We administered daily doses of 20 μg DT per kilogram body weight to WT, Lgr5-2A-DTR^{het}, and Lgr5-DTR-EGFP^{het} mice for 4 days and harvested the SI 6 h after the last DT dose (Figure 1B). *Lgr5* mRNA levels decreased by 92% and 65% in Lgr5-2A-DTR and Lgr5-DTR-EGFP SI from their respective untreated levels (Figure 1C). ISH confirmed that DT-treated Lgr5-2A-DTR and Lgr5-DTR-EGFP SI expressed visibly less *Lgr5* mRNA compared to their untreated counterparts and DT-treated WT SI (Figures 1D–1I). By H&E, control SI (DT-treated WT or untreated Lgr5-2A-DTR) displayed intact crypts, with CBCs intercalated by Paneth cells, whereas CBCs were largely absent in Lgr5-2A-DTR crypts after the first DT dose (Figure S1C). In addition, DNA fragmentation, characteristic of apoptosis, was observed in numerous Lgr5-2A-DTR crypt cells following the first DT dose. After 4 doses of DT, crypt integrity was severely compromised with the loss of CBCs and Paneth cells (Figure S1C). Caspase 3 staining confirmed that apoptotic cells were more abundant in Lgr5-2A-DTR crypts than Lgr5-DTR-EGFP crypts and absent in WT crypts (Figures 1J–1L).

To functionally determine the ablation efficiencies of the two DTR models, we crossed the DTR alleles onto the Lgr5-2A-CreERT2;Rosa26-tdTomato^{LSL} (Lgr5-2A-Cre;dTom) background to trace preexisting Lgr5^{+} ISCs and their progeny (Leushacke et al., 2017). Short-term tracing dynamics in Lgr5-2A-Cre;dTom SI recapitulated previous observations in the Lgr5-EGFP-ires-CreERT2 model (Barker et al., 2007), with dTom expression initially restricted to CBCs at 8 h following tracing initiation (reminiscent of Figures 1H and S1B), before expanding upward within 24 h (Figure S1D). Five days later, dTom tracing units encompassed the entire crypt-villus epithelium (Figure S1D).

The 2A models facilitate simultaneous lineage tracing and ablation treatments in healthy adult mice. Tracing was initiated in Lgr5-2A-Cre;dTom mice with or without Lgr5-2A-DTR/Lgr5-DTR-EGFP alleles using a single dose of tamoxifen followed by 4 daily doses of DT, and the SI then harvested 1 day after the first or last DT dose (Figures 1N and S1E). One day after 1 DT dose, dTom^{+} CBCs were readily observed in every crypt in control SI. In contrast, dTom signal was virtually absent from treated Lgr5-2A-DTR SI (Figure S1F). After 4 doses of DT, the control SI displayed dTom tracing in almost all crypts and villi (99.4% ± 0.3%; Figures 1O, 1P, and S1F), whereas minimal dTom signal was observed in DT-treated Lgr5-2A-DTR crypts (2.7% ± 0.7%) and villi (Figures 1O, 1Q, and S1F). These observations indicate ablation of almost all of the ISCs present immediately before the first DT treatment. In contrast, scattered dTom^{+} ribbons were readily seen in DT-treated Lgr5-DTR-EGFP crypts after a single DT dose; 25.9% ± 0.5% of crypts and associated villi expressed dTom after 5 days (Figures 1O, 1R, and S1G), demonstrating that some preexisting ISCs escaped ablation to generate progeny. Untreated Lgr5-2A-DTR and Lgr5-DTR-EGFP mice on a Lgr5-2A-Cre;dTom background behaved similarly to Lgr5-2A-Cre;dTom lacking a DTR allele (Figures S1D–S1G), indicating that inclusion of either DTR allele did not influence the SI dynamics. Thus, a near-complete ablation of Lgr5^{+} ISCs can be achieved using the Lgr5-2A-DTR model but not the Lgr5-DTR-EGFP model, even with daily DT administration. To understand the persistence of Lgr5^{+} ISC ablation in the Lgr5-2A-DTR model, we administered 2 doses of DT daily and harvested the mice after 4 days of recovery. By ISH, Lgr5 expression was efficiently re-established in these mice (Figure 1M), similar to previous observations (Tian et al., 2011). Lgr5 ISH signals were more intense than those in untreated mice (Figures 1H and 1M), suggesting a dynamic and robust response to Lgr5^{+} ISC ablation.

Frequent, efficient ablation of Lgr5^{+} ISCs in Lgr5-2A-DTR mice impairs intestinal homeostasis and function

After 4 daily doses of DT, Lgr5-2A-DTR SI were significantly shorter than WT SI (Figures 2A–2C) and displayed significant hemorrhaging, visible as dark intraluminal blood clots, which are absent in healthy WT SI (Figure 2B), and their villi were 33.3% shorter than those of WT SI (WT 688 ± 43 μm versus Lgr5-2A-DTR 459 ± 26 μm; Figures 2D–2F). DT-treated Lgr5-2A-DTR mice became moribund by the 4th or 5th DT dose when administered daily, while controls remained healthy. Lgr5-2A-DTR SI exhibited higher permeability than DT-treated WT SI in a 40-kDa dextran permeability assay after 3 daily doses of DT, before the mice showed any sign of being unwell (Figure 2G). These observations indicate a loss of epithelial integrity due to continuous Lgr5^{+} ISC ablation.

To examine the Lgr5^{+} ISC ablation phenotype in more detail, we profiled the transcriptomes of whole proximal SI from Lgr5-2A-DTR and WT mice after 4 daily DT doses by RNA sequencing (RNA-seq) (Figure 2D). A total of 3,189 differentially expressed genes (DEGs) were found (false discovery rate [FDR] < 0.05; Figure 2H; Table S1). Overrepresentation analysis using published markers of various epithelial and stromal populations in the SI (marker lists in Table S2) showed significantly reduced marker expression of differentiated Tuft cells, Paneth cells, and enterocytes, but not enteroendocrine, goblet, and most stromal populations in Lgr5-2A-DTR SI (Figures 2I and S2A). Analysis of a suite of Lgr5^{+} ISC markers (Muñoz et al., 2012) revealed a more complex picture; of the DEGs that were previously identified as ISC markers, Lgr5 (12.6-fold) and 19 other ISC marker genes were significantly downregulated, while 37 marker genes were

(J) Experimental timeline for (K)–(O).
(K) Representative images of dTom tracing in Axin2-2A-CreERT2;R26-dTom^{LSL} or Axin2-2A-CreERT2;R26-dTom^{LSL};Lgr5-2A-DTR at day 5.
(L) Quantification of proportion of villi displaying dTom tracing (n = 3/group).
(M) Clone sizes in Axin2-2A-CreERT2;RBW;Lgr5-2A-DTR (DTR) and Axin2-2A-CreERT2;RBW (WT) SI (n = 3/group). Black bars represent medians.
(N) Frequency of clones found in various parts of the crypts in each group. The statistics were analyzed by chi-square test.
(O) Representative images of DT-treated Axin2-2A-CreERT2;RBW;Lgr5-2A-DTR (DTR) and Axin2-2A-CreERT2;RBW (WT) SI.
Scale bars in (B) represent 1 cm, and those in (F), (K), and (O) represent 50 μm. Error bars represent SEMs.

significantly upregulated (Figure S1B; Table S2). Interestingly, *Ascl2* did not change significantly (FDR = 0.4) (Table S2). It was recently found that the expression of *Ascl2* precedes *Lgr5* in dedifferentiating cells (Murata et al., 2020), in line with the trend observed in RNA-seq results. There was no difference in *Olfm4* levels, another common ISC marker (Figure S2C). These mixed directionalities of changes in ISC markers likely reflect the transitional state of the dedifferentiating cells compensating for the Lgr5$^+$ ISC loss.

To validate the RNA-seq results, we performed ISH and immunostaining to identify the various populations found to be affected in the Lgr5-2A-DTR SI. Paneth cell numbers were reduced throughout the SI (Figure S2D), as previously observed (Metcalfe et al., 2014). The authors reasoned that the loss of Paneth cells was due to the bystander effect from apoptosis of Lgr5$^+$ ISCs, which cannot be attributed to a direct effect of Lgr5$^+$ ISC depletion. We also affirmed a clear reduction in the number of Tuft cells in Lgr5-2A-DTR SI (0.003 ± 0.003 per crypt section) compared to WT controls (0.68 ± 0.07 per crypt section) (Figure S2E). While morphological staining of two enterocyte markers, Alpi and Ezrin, did not show visible differences in signal intensities (Figures S2F and S2G), the downregulation of enterocyte markers in the Lgr5-2A-DTR samples likely reflects the reduced number of enterocytes within the shorter villi in Lgr5-2A-DTR SI (Figures 2D and 2E). In line with the RNA-seq results, the enteroendocrine (ChgA) population was not affected (Figures S2H and S2I). There was no significant enrichment of stromal markers among the DEGs, except for immune cells (Figures 2I, S2A, and S2B).

We analyzed the pathways affected by Lgr5$^+$ ISC ablation using Panther pathway and MSigDB. Cross-referencing the top 6 pathways from Panther analysis (Table S2) and MSigDB datasets with adjusted $p < 0.05$ (Table S2) highlighted overlaps in genes involved in Wnt pathway and chemokine/cytokine signaling. More detailed analysis revealed increased expression of genes positively associated with active Wnt signaling (e.g., Wnt10a, Myc, Tcf7l2, Edn1) and reduced expression of Wnt inhibitors (e.g., Sfrp5, Wnt5a, Pcdh20) in the Lgr5-2A-DTR SI, suggesting that Wnt/β-catenin signaling is upregulated upon Lgr5$^+$ ISC ablation, ostensibly as part of the dedifferentiation program. We sought to verify whether Wnt/β-catenin signaling was upregulated in the DT-treated Lgr5-2A-DTR SI via Axin2, a classical Wnt/β-catenin target gene. By ISH, while Axin2 expression is concentrated toward the WT crypt bases, DT-treated Lgr5-2A-DTR crypts exhibited broader, more uniform Axin2 expression throughout the crypt (Figures S2J and S2K), possibly accounting for the lack of change in Axin2 expression in the RNA-seq analysis. This indicates that more crypt cells have activated Wnt signaling in response to the ablation of Lgr5$^+$ ISCs. We also noted an enrichment of proliferation markers among the DEGs, all of which were upregulated in the DT-treated Lgr5-2A-DTR SI (Figures S2A and S2B), presumably to compensate for the loss of Lgr5$^+$ ISCs. However, Ki67 expression on tissue sections did not show visible differences (Figure S2M).

To determine any influence of Lgr5$^+$ ISC ablation on epithelial turnover, we generated Lgr5-2A-DTR;Axin-2A-CreERT2;dTom mice to label almost the entire crypt comprising ISCs and transit amplifying (TA) cells, excluding Paneth cells. We evaluated the rate of epithelial turnover by initiating tracing on day 1 and administering daily DT doses on days 1–4, and then measured the proportion of the villi length expressing dTom on days 3 and 5 (Figure 2J). The extent of tracing along the villi was reduced throughout DT-treated Lgr5-2A-DTR SI compared to controls by day 3 and was quantified in the proximal SI (24% ± 2% versus 37% ± 2%, respectively). This disparity was amplified by day 5 (58% ± 13% versus 100% ± 0% respectively, $p < 0.0001$) (Figures 2K, 2L, and S1), indicating that the loss of Lgr5$^+$ ISCs diminished the epithelial turnover rate. The reduced epithelial turnover in DT-treated Lgr5-2A-DTR SI is at odds with the increased proliferation suggested by the RNA-seq analysis of proliferation markers. There are two possible explanations for this: proliferation in the crypts is mainly geared toward regenerating new ISCs to replace the depleted ones while minimally contributing to new progeny in the villi, and/or migration of crypt progeny to villi is impaired.

To distinguish between the two scenarios, we performed clonal tracing (Red-Horse et al., 2010) using Axin2-2A-CreERT2;Rainbow;Lgr5-2A-DTR mice in the presence/absence of Lgr5$^+$ ISC ablation (Figure 2J). We made 3 striking observations: (1) single-colored clones in the DT-treated Axin-2A-CreERT2;RBW;Lgr5-2A-DTR SI crypts were generally larger than those in the DT-treated Axin-2A-CreERT2;RBW controls (average of 10.3 ± 6.4 cells per clone in DTR versus 5.5 ± 3.0 cells per clone in WT; Figures 2M and 2O); (2) in WT, ∼80% of monoclonal ribbons are restricted to the upper or lower halves of crypts, and ∼20% of these ribbons span both halves of the crypts; in DTR, 54.5% of the monoclonal ribbons traverse both halves of the crypts and minor proportions restricted to upper or lower halves of the crypts (Figures 2N and 2O); (3) both WT and DTR had similar proportions of monoclonal ribbons that extend from the upper halves of the crypts into the villus region (14.7% for DTR and 13.7% for WT), indicating that while crypt progeny migration to the villi is not blocked in Lgr5-2A-DTR SI, it is likely occurring at a lower rate in DTR compared to WT, in accordance with the results in Figures 2J–2L. These results suggest that ablating Lgr5$^+$ ISCs increases crypt proliferation to replenish cells at the crypt bases, likely originating from cells residing in the upper half of the crypts, and this proliferation does not directly contribute more differentiated cells entering the villi.

Lgr5+ ISCs are required for organoid initiation and survival

To further investigate the effect of ablating Lgr5$^+$ ISCs on the epithelium, we turned to *in vitro* epithelia-only organoids, which are maintained by Lgr5$^+$ ISCs (Sato et al., 2009). To determine whether Lgr5$^+$ ISCs are required to initiate organoids, we seeded crypts from WT, Lgr5-2A-DTR, and Lgr5-DTR-EGFP in the presence of DT and quantified the number of organoids that grew out on day 5 relative to the untreated counterpart (Figure 3A). While 0.05 μg/mL DT treatment did not affect WT organoid outgrowth (95.6% ± 7.2% of untreated WT organoids; Figures 3B, 3C, and 3F), only 7.2% ± 2.6% of plated Lgr5-2A-DTR crypts generated organoids (Figure 3B, 3D, and 3G), compared to 45.5% ± 6.2% outgrowth of Lgr5-DTR-EGFP crypts (Figures 3B, 3E, and 3H).

Separately, SI organoids from WT, Lgr5-2A-DTR, and Lgr5-DTR-EGFP SI were established for 5 days without DT, and

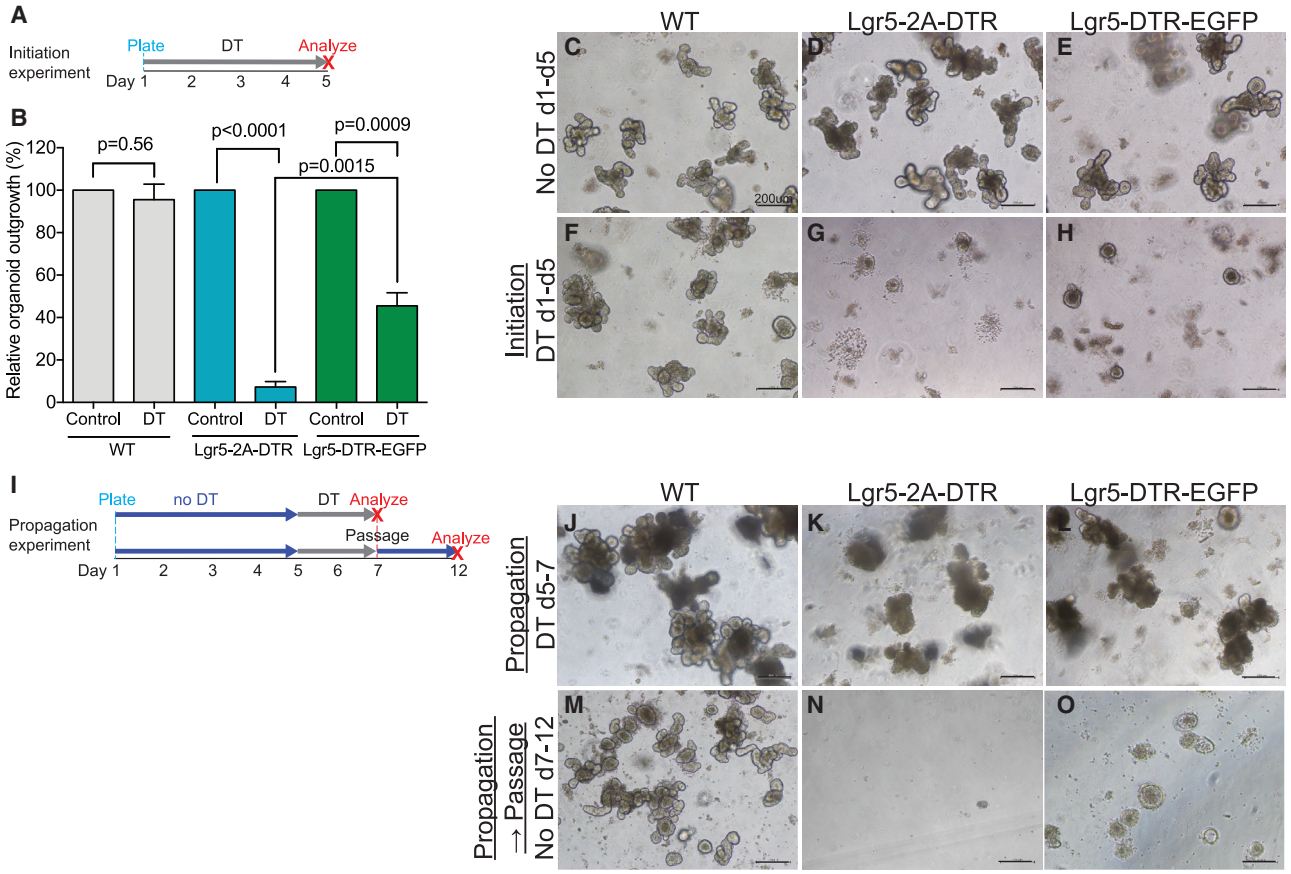

Figure 3. SI organoids require Lgr5$^+$ ISCs for initiation and survival

(A) Experimental timeline for (B)–(H).

(B) Relative percentages of organoids that grew out on day 5 of culture in the presence of 0.05 μg/mL DT (n = 3–4/group).

(C–H) Representative images of organoids in the conditions tested.

(I) Experimental timeline for (J)–(O).

(J–L) Representative images of organoids established in the absence of DT, then with 0.6 μg/mL DT from days 5 to 7 (n = 3/group).

(M–O) The organoids were passaged and cultured without DT from days 7 to 12.

Scale bars represent 200 μm. Error bars represent SEMs.

then cultured in DT from days 5 to 7 (Figure 3I). By day 7, while DT-treated WT organoids continued to grow, both DTR organoids began to disintegrate (Figures 3J–3L). In contrast to WT organoids, DT-treated Lgr5-2A-DTR organoids could not be passaged in culture medium lacking DT, while small cystic structures grew out from DT-treated Lgr5-DTR-EGFP organoids (Figures 3M–3O). These results demonstrate that Lgr5$^+$ ISCs are essential for organoid initiation and survival and further underscore the markedly lower ablation efficacy of Lgr5-DTR-EGFP compared to Lgr5-2A-DTR.

The more pronounced intestinal phenotype observed *in vitro* is likely a consequence of the relatively rapid clearance of DT *in vivo*, reducing the exposure of the resident Lgr5$^+$ ISCs relative to that achieved in organoids. To validate this, we seeded intestinal crypts in media containing DT, washed out the DT in media at various incubation lengths, and quantified organoid outgrowth and morphologies on day 5 (Figure 4A).

Compared to DT-treated WT organoids and untreated Lgr5-2A-DTR organoids, Lgr5-2A-DTR crypts transiently treated with DT could establish organoids, with the relative outgrowth rate decreasing with increasing exposure duration to DT (Figures 4B and 4D). These DT-treated Lgr5-2A-DTR organoid cultures comprised a mix of cystic and budded organoids, with the proportion of cystic organoids increasing with the length of DT exposure (Figures 4C and 4D). Cystic organoids are thought to be relatively immature, comprising more stem/progenitor cells with high Wnt signaling activity than their budding counterparts (Navis et al., 2019; Sato et al., 2011). To determine whether the cystic morphology was reversible, we treated newly plated SI crypts with DT for 6 h, washed out the DT, and passaged them in the absence of DT on day 5 (Figure 4E). More organoids reformed morphologically normal budded organoids (55.5% after passage [P1] versus 23% at initial plating [P0]) (Figure 4F). However, the proportion of morphologically normal budded organoids in this sample is still lower than that of WT organoids that received the same treatment (77.1%). The cystic organoids may represent a temporary regenerative state as a result of the damage

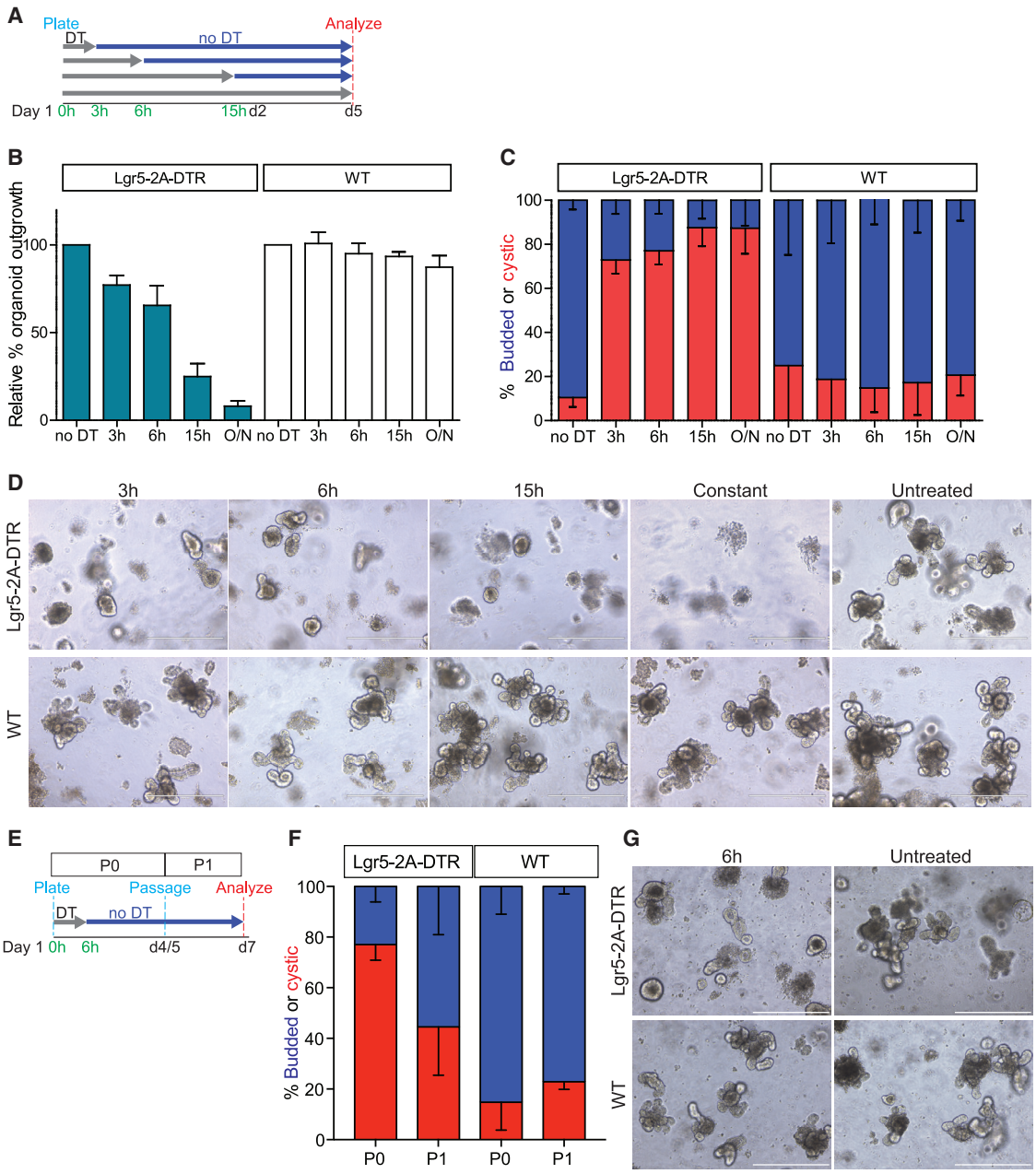

Figure 4. Organoid outgrowth efficiency reduces with increasing exposure to DT

(A) Experimental timeline for (B)–(D).

(B) Relative outgrowth rates for organoids treated with DT for various lengths of time (n = 5/group).

(C) Proportion of budded (>1 bud) or cystic organoids in each condition (n = 5/group).

(D) Representative images of organoids for all of the conditions tested.

(E) Experimental timeline for (F) and (G).

(F) Proportion of budded (>1 bud) or cystic organoids after passaging in each condition (n = 3/group).

(G) Representative images of organoids for all of the conditions tested.

Scale bars represent 400 μm. Error bars represent SEMs.

arising from Lgr5$^+$ ISC ablation. Therefore, the presence of DT in the organoid medium continuously ablates any reprogrammed Lgr5$^+$ ISCs, abrogating organoid growth. This indicates that the nascent Lgr5$^+$ ISCs derived from reprogrammed TA cells are required for organoid survival when preexisting Lgr5$^+$ ISCs are depleted, underscoring the need for a constant presence of Lgr5$^+$ ISCs for intestinal health and homeostasis.

DISCUSSION

The intestinal epithelium is thought to be resilient to acute loss of Lgr5$^+$ ISCs due to crypt plasticity, based on the lack of phenotype when Lgr5$^+$ ISCs are ablated using the existing Lgr5-DTR-EGFP mouse model (Murata et al., 2020; Tetteh et al., 2016; Tian et al., 2011; van Es et al., 2012). Using our highly efficient Lgr5-2A-DTR model, we found that a constant pool of Lgr5$^+$ ISCs is required for intestinal health and homeostasis. In the continual absence of Lgr5$^+$ ISCs, the intestinal epithelium starts to break down after a few days. Extension of these observations *in vitro* revealed that Lgr5$^+$ ISCs are essential for establishing and maintaining epithelial organoids. The prolonged absence of Lgr5$^+$ ISCs thus severely compromises the integrity of the intestinal epithelium.

The difference between our observations and earlier studies may be attributed to 2 factors: (1) our Lgr5-2A-DTR model achieves higher ablation efficiencies compared to the existing Lgr5-DTR-EGFP model, likely due to higher DTR expression levels, and (2) we administered DT daily *in vivo* to continuously ablate newly regenerated Lgr5$^+$ ISCs, which prevents Lgr5$^+$ ISC populations from re-establishing, in contrast to the alternate-day DT administration regimen used in previous studies. Since Paneth cells are niche cells supporting Lgr5$^+$ ISCs and can be reprogrammed to replenish lost ISCs (Jones et al., 2019; Sato et al., 2011; Schmitt et al., 2018; Yu et al., 2018), it is conceivable that the loss of these cells contributes to the phenotype observed in DT-treated Lgr5-2A-DTR mice, although the loss of Paneth cells under homeostatic conditions does not significantly impair epithelial renewal in the intestine (Durand et al., 2012). Importantly, any contribution of Paneth cell loss is highly unlikely to account for the phenotypic differences observed between the Lgr5-2A-DTR and Lgr5-DTR-EGFP mouse models, as the latter model also achieves near-complete loss of Paneth cells (Metcalfe et al., 2014).

The requirement for Lgr5$^+$ ISCs in epithelial maintenance was most pronounced in the organoids. Here, not only are newly reprogrammed Lgr5$^+$ cells rapidly eliminated in addition to pre-existing ones due to constant DT exposure but also the lack of stromal niche signals (Kabiri et al., 2014) could conceivably hamper the reprogramming capacity of non-Lgr5$^+$ cells. It is also possible that as organoid culture selects for cells that are highly reliant on R-spondin-amplified Wnt signaling, these cells would be more susceptible to Lgr5$^+$ ISC ablation and consequently present a more pronounced phenotype *in vitro*. We showed that organoids barely formed from Lgr5-2A-DTR crypts in the presence of DT, and established organoids could not survive after DT was added to the medium (Figure 3). Organoids established from the Lgr5-DTR-EGFP model also showed reduced fitness in the presence of DT, but they were less sensitive to DT than the Lgr5-2A-DTR organoids. These observations differ from published results (Tian et al., 2011) in which mature organoids were established from DT-treated Lgr5-DTR-EGFP mice in the presence of an unspecified concentration of DT. When we seeded crypts for organoid culture from DT-treated Lgr5-2A-DTR SI, we found that the crypts did not establish in the presence of DT *in vitro* (identical to results in Figure 3), but grew robustly in the absence of DT (data not shown), alluding to the prolific regeneration occurring in the crypts. Hence, the organoid data further substantiate our finding that Lgr5$^+$ ISCs are critical for epithelial maintenance.

The transient DT treatment *in vitro* suggests that non-Lgr5$^+$ progenitors are able to respond quickly to the loss of Lgr5$^+$ ISCs to reprogram and re-establish organoids. Hence, the alternate-day DT treatment used for animals in earlier studies may have provided sufficient time for new Lgr5$^+$ ISCs to form. Coupled with the reduced sensitivity of the Lgr5-DTR-EGFP model to DT, the alternate-day DT treatment yielded a subdued phenotype that was not detected in earlier homeostatic studies.

Another distinct consequence of Lgr5$^+$ ISC loss was the diminished rate of epithelial renewal (Figure 2). From the clonal tracing experiment using multicolor reporters, we surmise that crypt cells proliferate to replace ablated Lgr5$^+$ ISCs, with minimal contribution to differentiated cells migrating to the villi, thereby affecting epithelial renewal. If the mice could survive a longer regimen of DT dosing, we expect the SI epithelium to disintegrate. However, as the SI is a crucial organ for survival in nutrient absorption and maintaining a barrier between the body and external agents from ingested food, the increased permeability and bleeding observed in SI after 4 days of DT treatment were severe enough to cause mortality.

In conclusion, our results demonstrate that a constant pool of Lgr5$^+$ ISCs is required for intestinal homeostasis, and the SI cannot function in the face of persistent depletion of Lgr5$^+$ ISCs.

STAR★METHODS

Detailed methods are provided in the online version of this paper and include the following:

- KEY RESOURCES TABLE
- RESOURCE AVAILABILITY
  - Lead Contact
  - Materials Availability
  - Data and Code Availability
- EXPERIMENTAL MODEL AND SUBJECT DETAILS
  - Animals
  - Primary organoid cultures
- METHOD DETAILS
  - Administration of Tamoxifen and DT
  - Tissue processing and immunostaining (FFPE, IHC)
  - *In situ* hybridization (ISH)
  - Microscopy and image analysis
  - RNA processing for qPCR and sequencing
  - Organoid culture
  - Permeability assay
- QUANTIFICATION AND STATISTICAL ANALYSIS
  - Transcriptome analysis
  - Image quantification
  - qPCR analysis
  - Statistical analysis

Supplemental information

Supplemental Information can be found online at https://doi.org/10.1016/j.celrep.2020.108633.

ACKNOWLEDGMENTS

The authors thank IMB-IMU and the SBIC-Nikon Imaging Centre staff for imaging assistance; K. Murad for assistance with the experiments; G. Lim for manuscript assistance; and F. de Sauvage for providing the Lgr5-DTR-EGFP mice. N.B. is supported by the Agency for Science, Technology and Research (A*Star), the Japan Society for the Promotion of Science (JSPS) KAKENHI grant no. 17H01399, and the National Research Foundation Singapore (Investigatorship Program award no. NRF-NRF12017-03).

AUTHOR CONTRIBUTIONS

S.H.T. designed, performed all of the empirical experiments, collected and analyzed the data, and wrote the manuscript. P.P., S.Y., L.T.T., J.G., L.B.T., and M.C. performed the experiments and mouse husbandry. E.W., S.Y., and N.B. generated the transgenic mouse lines. B.L. analyzed the RNA-seq data. N.B. supervised the project, analyzed the data, and wrote the manuscript. All of the authors discussed the results and edited the manuscript.

DECLARATION OF INTERESTS

The authors declare no competing interests.

Received: May 11, 2020
Revised: September 9, 2020
Accepted: December 21, 2020
Published: January 26, 2021

REFERENCES

Barker, N., van Es, J.H., Kuipers, J., Kujala, P., van den Born, M., Cozijnsen, M., Haegebarth, A., Korving, J., Begthel, H., Peters, P.J., and Clevers, H. (2007). Identification of stem cells in small intestine and colon by marker gene Lgr5. Nature *449*, 1003–1007.

Durand, A., Donahue, B., Peignon, G., Letourneur, F., Cagnard, N., Slomianny, C., Perret, C., Shroyer, N.F., and Romagnolo, B. (2012). Functional intestinal stem cells after Paneth cell ablation induced by the loss of transcription factor Math1 (Atoh1). Proc. Natl. Acad. Sci. USA *109*, 8965–8970.

Haber, A.L., Biton, M., Rogel, N., Herbst, R.H., Shekhar, K., Smillie, C., Burgin, G., Delorey, T.M., Howitt, M.R., Katz, Y., et al. (2017). A single-cell survey of the small intestinal epithelium. Nature *551*, 333–339.

Jones, J.C., Brindley, C.D., Elder, N.H., Myers, M.G., Jr., Rajala, M.W., Dekaney, C.M., McNamee, E.N., Frey, M.R., Shroyer, N.F., and Dempsey, P.J. (2019). Cellular Plasticity of Defa4^{Cre}-Expressing Paneth Cells in Response to Notch Activation and Intestinal Injury. Cell. Mol. Gastroenterol. Hepatol. *7*, 533–554.

Kabiri, Z., Greicius, G., Madan, B., Biechele, S., Zhong, Z., Zaribafzadeh, H., Edison, Aliyev, J., Wu, Y., Bunte, R., et al. (2014). Stroma provides an intestinal stem cell niche in the absence of epithelial Wnts. Development *141*, 2206–2215.

Karpus, O.N., Westendorp, B.F., Vermeulen, J.L.M., Meisner, S., Koster, J., Muncan, V., Wildenberg, M.E., and van den Brink, G.R. (2019). Colonic CD90+ Crypt Fibroblasts Secrete Semaphorins to Support Epithelial Growth. Cell Rep. *26*, 3698–3708.e5.

Leushacke, M., Tan, S.H., Wong, A., Swathi, Y., Hajamohideen, A., Tan, L.T., Goh, J., Wong, E., Denil, S.L.I.J., Murakami, K., and Barker, N. (2017). Lgr5-expressing chief cells drive epithelial regeneration and cancer in the oxyntic stomach. Nat. Cell Biol. *19*, 774–786.

Metcalfe, C., Kljavin, N.M., Ybarra, R., and de Sauvage, F.J. (2014). Lgr5+ stem cells are indispensable for radiation-induced intestinal regeneration. Cell Stem Cell *14*, 149–159.

Mi, H., Muruganujan, A., Ebert, D., Huang, X., and Thomas, P.D. (2019). PANTHER version 14: more genomes, a new PANTHER GO-slim and improvements in enrichment analysis tools. Nucleic Acids Res. *47* (*D1*), D419–D426.

Muñoz, J., Stange, D.E., Schepers, A.G., van de Wetering, M., Koo, B.-K., Itzkovitz, S., Volckmann, R., Kung, K.S., Koster, J., Radulescu, S., et al. (2012). The Lgr5 intestinal stem cell signature: robust expression of proposed quiescent '+4' cell markers. EMBO J. *31*, 3079–3091.

Murata, K., Jadhav, U., Madha, S., van Es, J., Dean, J., Cavazza, A., Wucherpfennig, K., Michor, F., Clevers, H., and Shivdasani, R.A. (2020). Ascl2-Dependent Cell Dedifferentiation Drives Regeneration of Ablated Intestinal Stem Cells. Cell Stem Cell *26*, 377–390.e6.

Navis, M., Martins Garcia, T., Renes, I.B., Vermeulen, J.L., Meisner, S., Wildenberg, M.E., van den Brink, G.R., van Elburg, R.M., and Muncan, V. (2019). Mouse fetal intestinal organoids: new model to study epithelial maturation from suckling to weaning. EMBO Rep. *20*, e46221.

Red-Horse, K., Ueno, H., Weissman, I.L., and Krasnow, M.A. (2010). Coronary arteries form by developmental reprogramming of venous cells. Nature *464*, 549–553.

Sato, T., Vries, R.G., Snippert, H.J., van de Wetering, M., Barker, N., Stange, D.E., van Es, J.H., Abo, A., Kujala, P., Peters, P.J., and Clevers, H. (2009). Single Lgr5 stem cells build crypt-villus structures in vitro without a mesenchymal niche. Nature *459*, 262–265.

Sato, T., van Es, J.H., Snippert, H.J., Stange, D.E., Vries, R.G., van den Born, M., Barker, N., Shroyer, N.F., van de Wetering, M., and Clevers, H. (2011). Paneth cells constitute the niche for Lgr5 stem cells in intestinal crypts. Nature *469*, 415–418.

Schmitt, M., Schewe, M., Sacchetti, A., Feijtel, D., van de Geer, W.S., Teeuwssen, M., Sleddens, H.F., Joosten, R., van Royen, M.E., van de Werken, H.J.G., et al. (2018). Paneth Cells Respond to Inflammation and Contribute to Tissue Regeneration by Acquiring Stem-like Features through SCF/c-Kit Signaling. Cell Rep. *24*, 2312–2328.e7.

Seishima, R., Leung, C., Yada, S., Murad, K.B.A., Tan, L.T., Hajamohideen, A., Tan, S.H., Itoh, H., Murakami, K., Ishida, Y., et al. (2019). Neonatal Wnt-dependent Lgr5 positive stem cells are essential for uterine gland development. Nat. Commun. *10*, 5378–5394.

Subramanian, A., Tamayo, P., Mootha, V.K., Mukherjee, S., Ebert, B.L., Gillette, M.A., Paulovich, A., Pomeroy, S.L., Golub, T.R., Lander, E.S., and Mesirov, J.P. (2005). Gene set enrichment analysis: a knowledge-based approach for interpreting genome-wide expression profiles. Proc. Natl. Acad. Sci. USA *102*, 15545–15550.

Tetteh, P.W., Basak, O., Farin, H.F., Wiebrands, K., Kretzschmar, K., Begthel, H., van den Born, M., Korving, J., de Sauvage, F., van Es, J.H., et al. (2016). Replacement of Lost Lgr5-Positive Stem Cells through Plasticity of Their Enterocyte-Lineage Daughters. Cell Stem Cell *18*, 203–213.

Tian, H., Biehs, B., Warming, S., Leong, K.G., Rangell, L., Klein, O.D., and de Sauvage, F.J. (2011). A reserve stem cell population in small intestine renders Lgr5-positive cells dispensable. Nature *478*, 255–259.

van Es, J.H., Sato, T., van de Wetering, M., Lyubimova, A., Yee Nee, A.N., Gregorieff, A., Sasaki, N., Zeinstra, L., van den Born, M., Korving, J., et al. (2012). Dll1+ secretory progenitor cells revert to stem cells upon crypt damage. Nat. Cell Biol. *14*, 1099–1104.

Whitfield, M.L., George, L.K., Grant, G.D., and Perou, C.M. (2006). Common markers of proliferation. Nat. Rev. Cancer *6*, 99–106.

Yu, S., Tong, K., Zhao, Y., Balasubramanian, I., Yap, G.S., Ferraris, R.P., Bonder, E.M., Verzi, M.P., and Gao, N. (2018). Paneth Cell Multipotency Induced by Notch Activation following Injury. Cell Stem Cell *23*, 46–59.e5.

Zilionis, R., Engblom, C., Pfirschke, C., Savova, V., Zemmour, D., Saatcioglu, H.D., Krishnan, I., Maroni, G., Meyerovitz, C.V., Kerwin, C.M., et al. (2019). Single-Cell Transcriptomics of Human and Mouse Lung Cancers Reveals Conserved Myeloid Populations across Individuals and Species. Immunity *50*, 1317–1334.e10.

STAR★METHODS

KEY RESOURCES TABLE

REAGENT or RESOURCE	SOURCE	IDENTIFIER
Antibodies		
Rabbit monoclonal anti Ki-67	Thermo Scientific	MA5-14520; RRID AB_10979488
Rabbit polyclonal anti-RFP	Rockland	600-401-379; RRID:AB_2614911
Rabbit polyclonal anti-activated Caspase 3	Cell Signaling	9661, RRID:AB_2341188; RRID:AB_2341188
Rabbit polyclonal anti-Lysozyme	Dako	A0099; RRID:AB_2341230
Rabbit polyclonal anti-Ezrin	Abcam	Ab4069; RRID:AB_304261
Rabbit polyclonal anti-EGFP	Cell Signaling	2956S; RRID:AB_1196615
Mouse polyclonal anti-ChgA	Abcam	15160; RRID:AB_301704
Rabbit EnVision+	Dako	K4003; RRID:AB_2630375
Mouse EnVision+	Dako	K4001; RRID:AB_2827819
Chemicals, Peptides, and Recombinant Proteins		
Tamoxifen	Sigma	T5648; CAS:10540-29-1
Diphtheria toxin	Sigma	D0564
Critical Commercial Assays		
RNAscope® 2.5 HD Detection Reagents-BROWN	ACD	322310
FITC Dextran, 40kDa (Permeability assay)	Chondrex	4009
Intesticult Organoid Growth Medium (Mouse)	STEMCELL Technologies	06005
RNeasy Universal Plus Mini kit	QIAGEN	73404
Superscript III	ThermoFisher Scientific	18080093
Experimental Models: Organisms/Strains		
Mouse: C57BL/6J	InVivos	C57BL/6JInv
Mouse: Lgr5-2ACreERT2;R26Tdtom	Leushacke et al., 2017	N/A
Mouse: Lgr5-2A-DTR	Seishima et al., 2019	N/A
Mouse: Lgr5-DTR-EGFP	Tian et al., 2011	N/A
Mouse: Lgr5-EGFP-ires-CreERT2	Barker et al., 2007	N/A
Mouse: RBW	Red-Horse et al., 2010	N/A
Mouse: Axin2-2A-CreERT2	This paper	N/A
Mouse: Axin2-2A-EGFP	This paper	N/A
Oligonucleotides		
Lgr5 qPCR forward primer: AGAGCCTGATACCATCTGCAAAC	This paper	N/A
Lgr5 qPCR reverse primer: TGAAGGTCGTCCACACTGTTGC	This paper	N/A
Deposited Data		
RNA-seq	This paper	GSE148727
Other		
RNAscope® Probe- Mm-Lgr5	ACD	312171
RNAscope® Probe- Hs- HBEGF (DTR)	ACD	524821
RNAscope® Probe- Mm-Axin2	ACD	400331
RNAscope® Probe- Mm-Alpi	ACD	436781
RNAscope® Probe- Mm-Olfm4	ACD	311831
RNAscope® Probe- Mm-Dclk1	ACD	476631
RNAscope® Positive Control Probe- Mm-Ppib	ACD	313911

(*Continued on next page*)

Continued

REAGENT or RESOURCE	SOURCE	IDENTIFIER
RNAscope® Negative Control Probe- DapB	ACD	310043
RapiClear 1.52	Sunjin lab	RapiClear 1.52

RESOURCE AVAILABILITY

Lead Contact

Further information and requests for resources and reagents should be directed to and will be fulfilled by the lead contact, Nick Barker (Nicholas_barker@imcb.a-star.edu.sg).

Materials Availability

All unique/stable reagents generated in this study will be made available from the lead contact upon reasonable request, and may require a completed Materials Transfer Agreement.

Data and Code Availability

The accession number for the RNA-seq data reported in this study is GEO: GSE148727 (https://www.ncbi.nlm.nih.gov/geo/query/acc.cgi?&acc=GSE148727).

EXPERIMENTAL MODEL AND SUBJECT DETAILS

Animals

Mouse models used in this study were Lgr5-2A-CreERT, Lgr5-2A-DTR, Lgr5-EGFP-ires-CreERT2, Lgr5-DTR-EGFP, Axin2-2A-CreERT2, Axin2-2A-EGFP, Rosa26-tdTomato^{LSL}, Rosa26-Rainbow^{LSL}. All animal experiments were approved by the "Institutional Animal Care and Use Committee" of Singapore and performed in compliance with all relevant ethical regulations. For all experiments, adult animals (not selected for gender) with a minimum age of 7-8 weeks were used. The experiments were not randomized, and there was no blinded allocation during experiments and outcome assessment. No statistical method was used to pre-determine sample size.

Primary organoid cultures

Organoids were derived from SI of WT, Lgr5-2A-DTR and Lgr5-DTR-EGFP mice described above.

METHOD DETAILS

Administration of Tamoxifen and DT

The mice were injected with 133mg/kg tamoxifen and/or 20 μg/kg DT via intraperitoneal route.

Tamoxifen was first dissolved in ethanol, and an appropriate amount was combined with corn oil and evaporated in a vaccum centrifuge to remove the ethanol prior to injection. DT was dissolved in sterile PBS.

Tissue processing and immunostaining (FFPE, IHC)

IHC was performed according to standard protocols. In summary, tissues were fixed in 4% paraformaldehyde/PBS (w/v) overnight at 4°C, and processed into paraffin blocks. 8μm sections from the paraffin blocks and tissue microarray slides were deparaffinated and rehydrated, followed by antigen retrieval via heating to 121°C in a pressure cooker in commercial Tris/EDTA buffer pH 9.0 (S2367, DAKO). Primary antibodies used were rabbit anti-EGFP (1:200; Cell Signaling, 2956S), rabbit anti-Ki67 (1:200; Thermofisher, MA5-14520), rabbit anti-RFP (1:200; Rockland, 600-401-379), lysozyme (DAKOA0099),Cleaved Caspase 3(ASP 175)(Cell signaling, 9661) mouse anti-ChgA (1:200; Abcam, 15160), rabbit anti-Ezrin (1:00, Abcam, ab4069). The peroxidase-conjugated secondary antibodies used were mouse/rabbit EnVision+ (DAKO) for HRP IHC. IHC sections were dehydrated, cleared, and mounted with DPX (Sigma).

For whole mount imaging, tissues were fixed in 4% paraformaldehyde/PBS (w/v) overnight at 4°C, embedded in 4% low melting point agarose dissolved in PBS (w/v), and sectioned at 500μm thickness with VT1000 S vibratome (Leica). The sections were then permeabilized in 2% Triton X-100/PBS (v/v) O/N with Hoescht dye for nuclear stain. The next day, the sections were cleared in Rapiclear 1.52 (Sunjin lab) before imaging on the confocal microscope.

Immunostainings and imaging were performed on a minimum of three biological replicates and representative images of the replicates were included in the manuscript.

In situ hybridization (ISH)

ISH was performed using RNAscope 2.5 High Definition Brown Assay, according to manufacturer's instructions. DapB was used as negative control for all the RNAscope experiments. ISH and imaging were performed on a minimum of three biological replicates and representative images of the replicates were included in the manuscript.

Microscopy and image analysis

IHC and RNA ISH slides were imaged with Zeiss AxioImager Z1 upright microscope and Nikon Ri-2 upright microscope. Cultured organoids were imaged with Olympus DP-27 camera on Olympus IX53 inverted microscope. Whole mount tissues were imaged on Olympus FV3000RS inverted confocal microscope.

RNA processing for qPCR and sequencing

The proximal 3-5cm of the small intestines were lysed in Trizol (QIAGEN). RNA was subsequently isolated with RNeasy Universal Plus Mini kit (QIAGEN) and cDNA was generated with Superscript III (Life Technologies) according to manufacturer's instructions. qPCR was performed with a minimum of three biological replicates per gene using SYBR Green dye (Promega) according to the manufacturer's instructions and ran on StepOne or Quantstudio7 qPCR machines (Applied Biosystems).

Organoid culture

Briefly, dissociated crypts were resuspended in growth factor-reduced Matrigel (Corning) and cultured in STEMCELL Technologies' Intesticult media. DT was administered at 0.05 μg/ml for organoid initiation and 0.6 μg/ml for propagation cultures. For transient DT experiment, dissociated crypts were resuspended in growth factor-reduced Matrigel (Corning) and cultured in media with 0.05 μg/ml DT for stipulated times. The cultures were then washed in PBS thrice, and new Intesticult media without DT was added to the wells. Passaged organoids were cultured in Intesticult media without DT.

Permeability assay

Permeability assay was performed using FITC Dextran, 40kDa (Chondrex 4009) according to manufacturer's instructions. Mice were fasted for 4 hours before oral feeding and duration of experiment. FITC-Dextran was fed to the mice by oral gavage, blood sample was collected and fluorescence intensity read at Ex 490nm and Em 530nm with FITC Dextran standard curve on SpectraMax M5.

QUANTIFICATION AND STATISTICAL ANALYSIS

Transcriptome analysis

FASTQ files containing the RNA-Seq reads were checked for quality control issues using FASTQC and MultiQC for which no issues were found. The reads were then mapped to the mouse genome build mm10 using STAR based on GENCODE M22 annotations. Gene counts were counted using featureCounts (part of the Subread package) based on GENCODE M22 annotations. The gene counts were then used in edgeR for a differential expression of genes (DEG) analysis comparing DTR and WT samples with multiple testing correction done using the method of Benjamini and Hochberg.

GSEA analysis was done the fgsea bioconductor package using gene sets obtained from the Molecular Signatures Database (Subramanian et al., 2005), and pathway enrichment was performed using PANTHER version 14 (Mi et al., 2019). Since the reads are from mouse, ENSEMBL Compara (based on ENSEMBL Genes 99) was used to map the mouse genes to human genes prior to analysis.

Gene Ontology enrichment analysis was done using the topGO bioconductor packages.

Gene set enrichment against the various gene sets were done using Fisher's Exact tests. Markers for various populations used in overrepresentation analysis were obtained from the following references: Tuft, Paneth, enterocytes, goblet, enteroendocrine cells (Haber et al., 2017); ISCs (Muñoz et al., 2012); stromal fibroblasts (Karpus et al., 2019); endothelial cells ("Endothelial Cell Markers," https://www.rndsystems.com/research-area/endothelial-cell-markers); smooth muscle cells ("Smooth Muscle Cell Markers," https://www.rndsystems.com/research-area/smooth-muscle-cell-markers); nerves ("Neural Cell Markers," https://resources.rndsystems.com/images/site/rnd-systems-neural-markers-br2.pdf); immune cells (healthy mouse lung transcriptomics from Zilionis et al., 2019); proliferation (Whitfield et al., 2006).

All analyses were done using R version 3.6.2 and P values less than 0.05 were considered to be significant.

Image quantification

Images were analyzed and processed using ImageJ (NIH). Measurements for villi lengths, clonal counts and dTom tracing lengths were done with ImageJ. Villi lengths and clonal counts were sampled across the proximal third of the small intestines, while dTom tracing lengths were sampled across the entire length of the small intestine.

qPCR analysis

Analysis was carried out using double CT method on Step One Software on the respective qPCR machines (Applied Biosystems).

Statistical analysis

All statistical analyses were performed with at least 3 biological replicates, using two-sided unpaired Student's t test, unless otherwise stated, and analyzed on Prism software.